Energy Materials

Supplementary Materials

Polyethylene glycol with hydroxylated ammonium polyphosphate flame-retardant phase change composites for thermal storage

Ruifeng He[1], Xiaowei Wu[1], Xuxiong Li[1], Peihui Chen[1], Junting Shi[2], Weifu Xu[3], Canbing Li[4], Xinxi Li[1,*]

[1]School of Materials and Energy, Guangdong University of Technology, Guangzhou 510006, Guangdong, China.

[2]Inner Mongolia Research Institute, Shanghai Jiao Tong University, Hohhot 010010, Inner Mongolia, China.

[3]Shenzhen DEM Technology Co., Ltd., Shenzhen 518107, Guangdong, China.

[4]Department of Electrical Engineering, Shanghai Jiao Tong University, Shanghai 200240, China.

[*]**Correspondence to:** Prof. Xinxi Li, School of Materials and Energy, Guangdong University of Technology, Guangzhou 510006, Guangdong, China. E-mail: pkdlxx@gdut.edu.cn

S1. Comparison with previously reported phase-change materials

Table S1 compares the thermal conductivity, latent heat, anti-leakage performance, and peak heat release rate (PHRR) of the CPCM developed in this work with those of representative solid–solid or form-stable phase-change materials reported in the literature. The PEG/HDI/HAPP/EG composite developed in this study exhibits a thermal conductivity of 1.547 W/(m·K), a latent heat of 111.35 J/g, and a mass retention of 99.88%, demonstrating a favorable balance among heat-transfer capability, thermal-energy-storage capacity, and shape stability. The PHRR data are also included to provide a comparison of the combustion behavior. However, because the material formulations, sample dimensions, and testing conditions differ among the cited studies, the values should be regarded as a general performance comparison rather than a strictly quantitative ranking.

Table S1. Comparison of the thermal conductivity, latent heat, anti-leakage performance, and peak heat release rate of different phase-change materials reported in the literature and developed in this work

Sample	Thermal Conductivity (W/(m·K))	Latent heat (J/g)	Anti-leakage	PHRR (KW/m^2)	Source
PEG/MDI/DMG	0.78	91.7	100	-	[1]
PEG/MDI/OMMT	0.30	106.8	98.12	-	[2]
PEG/MDI/HA/HCCP	1.29	120.4	100	610	[3]
Vanillin/ODA/DEP	0.21	59.2	0	144.8	[4]
PEG/PGI/APP/BPO	0.38	70.1	98.1	413	[5]
PEG/HDI/HAPP/EG	1.547	111.35	99.88	647.04	This Work

Note: Anti-leakage performance is expressed as the mass retention after the leakage test. PHRR denotes the peak heat release rate. "–" indicates that the corresponding value was not reported in the cited reference. Owing to differences in test methods

and experimental conditions, direct comparison of the reported values should be interpreted with caution.

[1] J. Zhong, J. Zhang, Y. Wang, H. Fan, X. Meng, X. Feng, J. Yan, Preparation and performance characterisation of a physically and chemically crosslinked self-healing phase change material, Journal of Energy Storage, 130 (2025) 117470.

[2] N. Gao, T. Tang, H. Xiang, W. Zhang, Y. Li, C. Yang, T. Xia, X. Liu, Preparation and structure-properties of crosslinking organic montmorillonite/polyurethane as solid-solid phase change materials for thermal energy storage, Solar Energy Materials and Solar Cells, 244 (2022) 111831.

[3] T. Wang, J. Deng, J. Du, W. Yang, Y. Zeng, T. Wu, Z. Rao, X. Li, Investigation on the polyethylene glycol based composite phase change materials with coating flame-retardant for battery thermal management, Case Studies in Thermal Engineering, 65 (2025) 105616.

[4] S. Wang, G. Zhang, Y. Zhang, Bio-based intrinsic flame-retardant phase change material derived from vanillin, Journal of Energy Storage, 125 (2025) 116987.

[5] G.-Z. Yin, X.-M. Yang, J. Hobson, A.M. López, D.-Y. Wang, Bio-based poly (glycerol-itaconic acid)/PEG/APP as form stable and flame-retardant phase change materials, Composites Communications, 30 (2022) 101057.

S2. XRD characterization of expanded graphite

As depicted in Fig. S1, the sharp and intense diffraction peak at approximately 26° corresponds to the (002) crystal plane of graphitic carbon, indicating a highly graphitized crystalline structure.

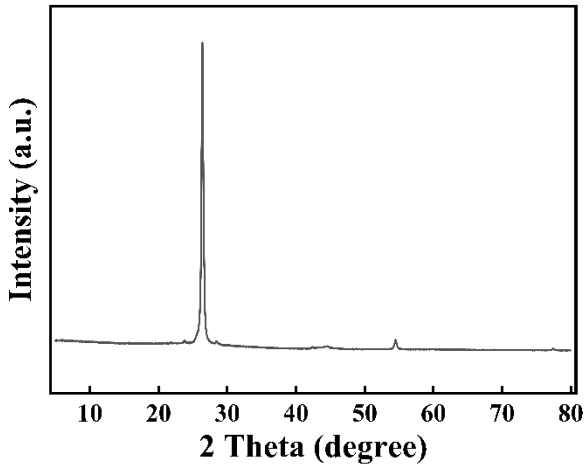

Fig. S1. XRD patterns of EG.

S3. Statistical analysis of melting enthalpy

To evaluate the reproducibility of the phase-change enthalpy measurements, the melting enthalpies of PEG and the CPCMs were determined from three independent DSC measurements. The results are presented as the mean ± standard deviation (SD), as summarized in Table S2. These mean values and corresponding standard deviations were used to construct the phase-change enthalpy data and error bars in Fig. 4(b) of the main manuscript.

The mean melting enthalpy of PHHE was determined to be 111.35 ± 4.32 J/g (n = 3). By comparison, the value of 111.97 J/g reported in the thermal-cycling experiment corresponds to the initial melting enthalpy of the specific PHHE specimen subjected to 100 heating–cooling cycles. This value was not included in the calculation of the mean and standard deviation reported in Table S2. The difference of 0.62 J/g between the two values lies within the standard deviation of the three independent measurements. Therefore, the two values represent different data sets rather than

inconsistent measurements.

Table S2. Melting enthalpies of PEG and the CPCMs obtained from three independent DSC measurements

Sample	Melting enthalpy, ΔH_m (J/g)	Number of measurements
PEG	164.25 ± 3.87	3
PH	131.75 ± 3.75	3
PHE	115.21 ± 4.20	3
PHA	107.04 ± 4.56	3
PHAE	92.04 ± 3.56	3
PHH	119.75 ± 4.98	3
PHHE	111.35 ± 4.32	3

S4. Crystallization behavior of PEG and different CPCMs

Further insight into the crystallization behavior of PEG and the different CPCMs was obtained from the DSC cooling curves shown in Fig. S2. The crystallization peak temperature (T_c), crystallization enthalpy (ΔH_c), and relative crystallinity (X_c) are quantitatively summarized in Table S3. The relative crystallinity was calculated by normalizing the crystallization enthalpy to the PEG2000 content of each sample and using pure PEG measured under the same conditions as the reference. Pure PEG exhibits a crystallization peak temperature of 24.67 °C and a crystallization enthalpy of 155.38 J/g. The CPCMs show crystallization peak temperatures ranging from 27.33 to 28.83 °C. Although their crystallization enthalpies are lower than that of pure PEG because of the presence of non-phase-change components, the PEG-content-normalized results show that the relative crystallinities range from 76.15% to 96.64%.

The incorporation of EG causes modest, composition-dependent changes in the crystallization behavior. The relative crystallinity decreases from 90.74% for PH to 83.92% for PHE and from 83.68% for PHA to 76.15% for PHAE, indicating that EG

and the crosslinked network restrict the ordered packing of PEG chains. In contrast, PHH and PHHE maintain relatively high crystallinities of 96.64% and 93.12%, respectively. In particular, PHHE exhibits the highest relative crystallinity among the EG-containing CPCMs, demonstrating that the HAPP-containing network provides structural confinement while retaining favorable crystallization capability. This result is consistent with the high latent-heat-storage performance of PHHE.

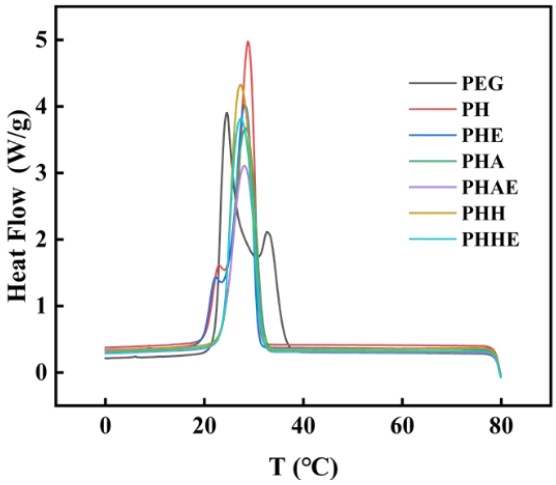

Fig. S2. DSC crystallization curves of different samples.

Table S3. Crystallization parameters and relative crystallinity of PEG and different CPCMs

Sample	PEG2000 content (wt%)	Crystallization peak temperature, T_c (°C)	Crystallization enthalpy, ΔH_c (J/g)	Relative crystallinity, X_c (%)
PEG	100.00	24.67	155.38	100.00
PH	92.24	28.83	130.05	90.74
PHE	87.63	28.17	114.27	83.92
PHA	77.94	28.33	101.34	83.68
PHAE	74.05	28.17	87.62	76.15
PHH	77.94	27.33	117.03	96.64

PHHE	74.05	27.50	107.14	93.12

Note: T_c was determined from the maximum of the exothermic crystallization peak, and ΔH_c was obtained by integrating the crystallization peak. The relative crystallinity was calculated according to:

$$X_c = \frac{\Delta H_{c,sample}}{w_{PEG} \times \Delta H_{c,PEG}} \times 100\% \quad \text{(S1)}$$

where w_{PEG} is the mass fraction of PEG2000 in each sample, and $\Delta H_{c,PEG}$ is the crystallization enthalpy of pure PEG measured under the same conditions.

S5. Thermal-cycling stability and anti-leakage performance of PHHE

The long-term thermal reliability of PHHE was evaluated through DSC cycling and macroscopic heating–cooling tests. For the DSC test, an approximately 8.0 ± 0.1 mg sample was repeatedly heated from 30 to 80 °C at 10 °C/min and cooled back to 30 °C under a nitrogen flow of 50 mL/min. A total of 100 heating–cooling cycles were performed.

As shown in Fig. S3 and Table S4, the melting peak temperature remained nearly unchanged at approximately 54.3 °C throughout the cycling process. The melting enthalpy decreased slightly from 111.97 J/g before cycling to 111.19 J/g after 100 cycles, corresponding to an enthalpy retention of 99.30%. This minor variation demonstrates the excellent phase-transition stability of PHHE.

PHHE was also subjected to 100 macroscopic heating–cooling cycles between 30 and 80 °C in a temperature-controlled chamber, with a heating rate of 3 °C/min. As shown in Fig. S4, no visible leakage or structural deformation was observed after cycling, and the mass retention reached 99.91%. These results confirm that PHHE possesses favorable thermal-cycling durability and shape stability.

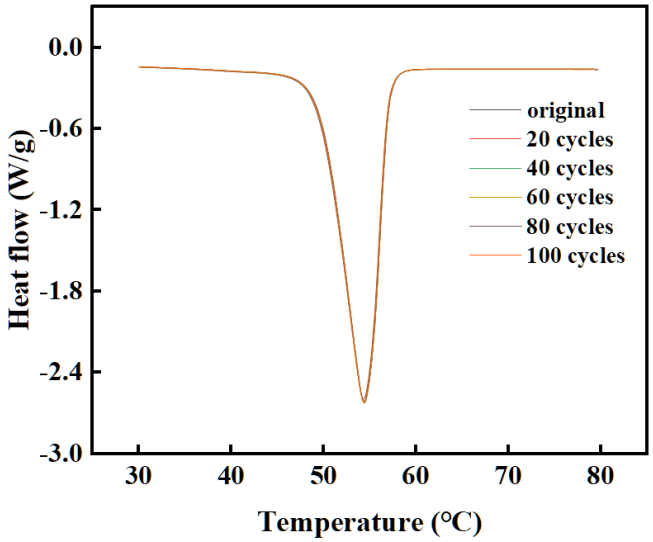

Fig. S3. DSC heating curves of PHHE before cycling and after 20, 40, 60, 80, and 100 heating–cooling cycles.

Table S4. The melting temperature and latent heat value of PHHE undergoing different cycle times during the heating process

Cycles	Heating Process	
	T_m (°C)	Latent Heat (J/g)
Original	54.3	111.97
20	54.3	111.71
40	54.3	111.61
60	54.3	111.44
80	54.3	111.32
100	54.3	111.19

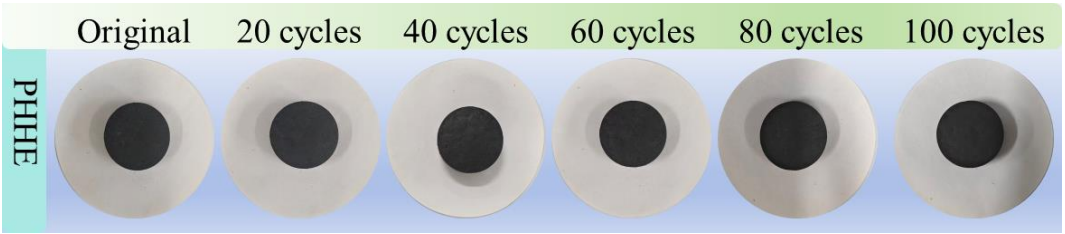

Fig. S4. Digital photographs of PHHE after 0, 20, 40, 60, 80, and 100 heating–cooling cycles between 30 and 80 °C, showing its anti-leakage performance and shape stability.

S6. Apparent photothermal conversion efficiency

The apparent photothermal conversion efficiency of the CPCMs was calculated from the latent heat stored during the phase-transition process. The phase-transition time, Δt, was determined from the photothermal heating curve as the time required for the sample temperature to pass through the corresponding phase-transition range obtained from the DSC results. The apparent photothermal conversion efficiency was calculated according to Eq. (2) in the main text.

The phase-transition time, Δt, was determined from the photothermal heating curve as the time required for the sample temperature to pass through the corresponding DSC-derived phase-transition range. In Eq. (2), m is the sample mass, ΔH_m is the melting enthalpy, I is the incident light intensity (0.15 W/cm^2), and A is the irradiated surface area. The calculation parameters and apparent photothermal conversion efficiencies are summarized in Table S5.

Table S5. Calculation parameters and apparent photothermal conversion efficiencies of the CPCMs

Sample	Phase-transition range (°C)	Δ*t* (s)	*A* (cm^2)	m (g)	Δ*H*$_m$ (J/g)	*η* (%)
PHE	50.84-58.60	211.01	4.854	0.9531	115.21	71.47
PHAE	53.04-58.49	182.27	4.305	0.9340	92.04	73.04
PHHE	50.00-59.53	491.50	3.420	1.6693	111.35	73.72

S7. Thermocouple Arrangement and Temperature Difference Calculation

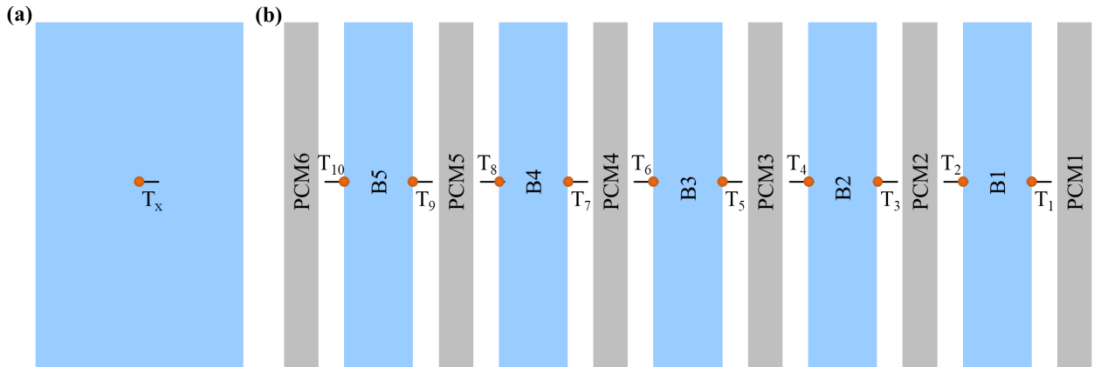

Fig. S5. Thermocouple arrangement in the battery module: (a) thermocouple position on the battery surface; (b) front view of the thermocouple distribution.

As shown in Fig. S5, the battery module consisted of five cells, denoted as B1–B5, and six CPCM layers, denoted as PCM1–PCM6. Two thermocouples were attached to the centers of the two major surfaces of each cell at the cell–CPCM interfaces. Therefore, ten temperature measurement points, labeled T_1–T_{10}, were used for each battery module. The thermocouple positions were identical for the PHE-Module, PHAE-Module, and PHHE-Module.

At each time point, the maximum and minimum temperatures of the module were determined as:

$$T_{max}(t) = \max\{T_1(t), T_2(t), \dots, T_{10}(t)\} \quad \text{(S2)}$$

$$T_{min}(t) = \min\{T_1(t), T_2(t), \dots, T_{10}(t)\} \quad \text{(S3)}$$

The instantaneous temperature difference was calculated as:

$$\Delta T(t) = T_{max}(t) - T_{min}(t) \quad \text{(S4)}$$

The maximum temperature difference during one charge–discharge cycle was determined as:

$$\Delta T_{max} = max\,[\Delta T(t)] \quad \text{(S5)}$$

This calculation was used to evaluate and compare the temperature uniformity of the three battery modules.